

Interstellar medium disruption in the Centaurus A group

Antoine Bouchard¹

*Research School of Astronomy & Astrophysics, Mount Stromlo Observatory, Cotter Road,
Weston Creek, ACT 2611 Australia*

and

Australia Telescope National Facility, PO Box 76, Epping, NSW 1710, Australia

bouchard@obs.univ-lyon1.fr

Helmut Jerjen

*Research School of Astronomy & Astrophysics, Mount Stromlo Observatory, Cotter Road,
Weston Creek, ACT 2611 Australia*

Gary S. Da Costa

*Research School of Astronomy & Astrophysics, Mount Stromlo Observatory, Cotter Road,
Weston Creek, ACT 2611 Australia*

Jürgen Ott²

Australia Telescope National Facility, PO Box 76, Epping, NSW 1710, Australia

ABSTRACT

We present the results of a 21 cm neutral hydrogen (HI) line detection experiment in the direction of 18 low luminosity dwarf galaxies of the Centaurus A group, using the Australia Telescope National Facility 64m Parkes Radio Telescope and the Australia Telescope Compact Array. Five dwarfs have HI masses between $M_{\text{HI}} = 4 \times 10^5$ to $M_{\text{HI}} = 2.1 \times 10^7 M_{\odot}$ and $0.04 < M_{\text{HI}}/L_{\text{B}} < 1.81 M_{\odot} L_{\odot, \text{B}}^{-1}$. The other 13 have upper-limits between $M_{\text{HI}} < 5 \times 10^5$ and $M_{\text{HI}} < 4 \times 10^6 M_{\odot}$ ($M_{\text{HI}}/L_{\text{B}} < 0.24 M_{\odot} L_{\odot, \text{B}}^{-1}$). Two of the mixed-morphology dwarfs remain undetected in HI, a situation that is in contrast to that of similar Local Group and Sculptor group objects where all contain significant amounts of neutral gas. There is a discontinuity in the HI properties of Centaurus A group low luminosity dwarfs that is unobserved amongst Sculptor group dwarfs. All objects fainter than $M_{\text{B}} = -13$ have either $M_{\text{HI}} > 10^7 M_{\odot}$ or $M_{\text{HI}} < 10^6 M_{\odot}$. This gap may be explained by the ram pressure stripping mechanism at work in this dense environment where all galaxies with $M_{\text{HI}} < 10^7 M_{\odot}$ have been stripped of their gas. The required intergalactic medium density to achieve this is $\sim 10^{-3} \text{ cm}^{-3}$.

Subject headings: galaxies: groups: individual(Centaurus A) — galaxies: dwarfs
 — galaxies: evolution — galaxies: ISM

1. Introduction

Galaxy morphology is a static description of an evolving stellar system. It is the visual manifestation of the physical processes that shaped the global optical light distribution over a Hubble time. It is the present day star formation, generating discreet pockets of young bright stars and H II regions, that leads to the irregular B-band appearance of late-type dwarfs. Star formation activity, however, can only operate until the resources for producing new stars in the form of neutral hydrogen reservoirs, is exhausted. This eventually results in an object with a smooth, featureless light distribution (an early-type dwarf), devoid of any significant amount of interstellar medium (ISM). Whether or not these evolved late-type galaxies will have the same properties as the present day early-type dwarf galaxies is a much discussed matter (Mayer et al. 2001; Pedraz et al. 2002; Simien & Prugniel 2002; Grebel et al. 2003; De Rijcke et al. 2003, 2004; van Zee et al. 2004; Read & Gilmore 2005). The evolutionary phase between the two major morphological types provides observable objects (known as transition-type dwarfs, dE/dIrr) with a continuum in both gas and stellar properties between the two extremes: gas rich dwarf Irregulars (dIrr) and gas poor dwarf Ellipticals (dE, also incorporating dwarf Spheroidals, dSph and dwarf S0s, dS0).

In essence, to be classified as “early-type”, a dwarf galaxy only needs to have had no recent star formation. This could, in principle be independent of the presence or absence of H I gas. Indeed, while the Local Group dEs exhibit a wide variety of star formation histories (e.g., Grebel 2001), few show signs of recent star formation (Tolstoy et al. 2004; Babusiaux et al. 2005; Olszewski et al. 2006) yet some are not completely devoid of H I. The two early-type galaxies companions to M31, NGC185 and NGC205 (Young & Lo 1997) and the Sculptor dSph (Carignan et al. 1998; Bouchard et al. 2003) are examples (see also Blitz & Robishaw 2000) where traces of H I are detected ($M_{\text{HI}} \sim 10^5 M_{\odot}$). Moreover, all known Local Group transition type galaxies have been detected in H I: LGS3 contains $M_{\text{HI}} = 6 \times 10^5 M_{\odot}$ (Young & Lo 1997; Robishaw et al. 2002), Phoenix has $1 \times 10^5 M_{\odot}$ (St-Germain et al. 1999; Gallart et al. 2001), Antlia has $7 \times 10^5 M_{\odot}$ (Barnes et al. 2001),

¹Current address: Université de Lyon 1, Centre de Recherche Astronomique de Lyon, Observatoire de Lyon, 9 avenue Charles André, F-69230 Saint-Genis Laval, France; CNRS, UMR 5574 ; École Normale Supérieure de Lyon, Lyon, France.

²Bolton Fellow

DDO210 has $2 \times 10^6 M_{\odot}$ and Pegasus has $5 \times 10^6 M_{\odot}$ (Lo et al. 1993). The same observation is made for the four known transition type galaxies of the Sculptor group; these have $3 \times 10^5 M_{\odot} < M_{\text{HI}} < 10^6 M_{\odot}$ (Bouchard et al. 2005). Two dS0 galaxies ESO384-G016, in the Centaurus A group, and NGC 59, in the Sculptor group, have also been detected with $M_{\text{HI}} > 10^6 M_{\odot}$ (Beaulieu et al. 2006). Similarly, in galaxy clusters, up to 15% of early-type dwarfs still have substantial amounts of HI ($M_{\text{HI}} \gtrsim 10^7 M_{\odot}$ Conselice et al. 2003). It is therefore incorrect to believe that only currently star forming or irregular galaxies contain ISM.

The detection of HI in early-type dwarf galaxies is an important step in understanding any morphological evolution scenario. Gas depletion is still viewed as the key factor driving the transition from late to early-type (e. g., Conselice et al. 2003). Morphological properties of galaxies are strongly correlated to their environment (Dressler 1980; Binggeli et al. 1987, 1990; van den Bergh 1994) and factors such as ram pressure (Einasto et al. 1974) and tidal fields (Moore et al. 1996), galactic winds (Marcolini et al. 2004) and enhanced star formation efficiency (Buyle et al. 2005) can, in principle, remove or exhaust the gas from a late-type dwarf and force the transition. However, since ISM is detected in some early-type dwarfs, there are other options one needs to study. (1) Gas depletion is not an end state, i. e., gas can be accreted from various sources such as stellar winds, intergalactic medium, etc. (e. g., Mould et al. 1990). (2) The gas is not depleted but is difficult to detect; e. g., the ISM resides in an ionised state (Mashchenko et al. 2004). In these cases, dEs may still have the means to form new stars and thus to oscillate between morphologies: some could be quiescent mixed-morphology dwarfs.

By identifying and analysing low mass dwarf galaxies that contain HI, we can constrain this theory of evolution. For the Local Group, the work has been conducted by Blitz & Robishaw (2000) and Bouchard et al. (2006) who have identified a number of early-types dwarfs possibly associated with HI emission. In the Sculptor group, only one ‘genuine’ early-type dwarf, i. e., one without any detected ISM, could be found (Bouchard et al. 2005), in accordance with morphological predictions (Jerjen et al. 2000b). This makes the Sculptor group one of the rare environments where late-type dwarfs vastly outnumber early-types: for example, down to $M_B \sim -10$, Sculptor has one early-type dwarf against 18 late-types (Côté et al. 1997, hereafter CFC97; Karachentseva & Karachentsev 1998, hereafter KK98; Jerjen et al. 2000b) while the Local Group has at least 17 early-type dwarfs against 16 late-type dwarfs (Mateo 1998). The Sculptor group has an elongated shape extending over ~ 3 Mpc (Jerjen et al. 1998; Karachentsev et al. 2004) and is therefore more of a galaxy ‘cloud’ than a gravitationally bound entity; it does not have high galaxy density regions. This makes environmental influences such as ram pressure and tidal stripping largely ineffective and may explain the lack of early-type objects.

The Centaurus A (CenA) group is a much denser environment than Sculptor. CFC97 identified ~ 20 dIrr galaxies in the CenA group using photographic plates as well as HI and H α spectroscopy. In a complementary study, 13 dwarf galaxy candidates of early and mixed morphology were detected by Jerjen et al. (2000a), five of which had their distances measured and membership confirmed by the surface brightness fluctuation technique (Jerjen et al. 2000b). Several other catalogs and studies describing galaxies of the CenA group have also been published (KK98; Banks et al. 1999; Karachentseva & Karachentsev 2000; Karachentsev et al. 2002, 2006). In total, the CenA group contains at least 54 galaxies and has NGC5128 (CenA) and NGC5236 (M83) at the center of its principal density peaks. Of this number, ~ 50 galaxies are dwarfs (with absolute B magnitude fainter than $M_B > -18$): 32 are late-type, 14 are early-type and 4 are of mixed-morphology. This rich group environment is, after Sculptor, the next logical target to search for HI rich dEs.

This paper presents the results of Parkes single-dish and Australia Telescope Compact Array HI observations in the direction of 18 CenA dwarf galaxies. The aim was to obtain a complete picture of HI properties in all known CenA group dwarf galaxies to a low HI mass limit. The following pages are divided as follow: Section 2 contains information on the target selection and observations. The main results of this investigation are found in Section 3 while the analysis and implications are discussed in Section 4. Finally Section 5 presents the conclusions of the paper.

2. Observations

2.1. Sample selection

The CenA galaxy group (Figure 1) was chosen because it represents a widely different environment to the low density Sculptor group, which we studied earlier (Bouchard et al. 2005). The relatively large number of galaxies, the presence of an active radio galaxy (CenA) and the high overall density of the group makes it more akin to a cluster environment. The biggest advantage of the CenA group, however, is its short distance to the Milky Way (~ 4.1 Mpc), which makes deep and detailed HI studies of its members possible.

Our aim is to study the HI properties of galaxies that are the most susceptible to mass-loss mechanisms. These mechanisms will operate most effectively at the faint-end of the galaxy luminosity function. From the lists compiled by CFC97, Jerjen et al. (2000a), KK98, and Karachentsev et al. (2006), we see that the CenA group contains 35 known dwarfs with $M_B \gtrsim -14$ (14 early-type, 17 late-type and 4 mixed type) and, of these, we observed 18: 10 early-type, four late-type and all four mixed-type. The properties of these dwarfs, i. e.,

the morphological types, spatial positions, radial distances, apparent magnitudes, Galactic extinctions, and optical heliocentric radial velocities, are summarised in Table 1. While all these galaxies have previously been observed with HIPASS (Barnes et al. 2001), that all-sky survey lacked sufficient resolution or sensitivity to constrain the properties of these low mass objects. They were re-observed with either the Parkes Radio Telescope or the Australia Telescope Compact Array.

2.2. Parkes observations

Using the same approach as Bouchard et al. (2005), the 64m Parkes Telescope³ was employed to obtain high spectral resolution HI line spectra in the direction of the early-type dwarfs AM1343-452, ESO269-G066, CenA-dE1 and CenA-dE4. The observations were conducted in February 2005 (project P475). The Multibeam instrument in MX (beam-switching) mode and the narrowband correlator with the MB7_8_2048 settings, provided a bandwidth of 8 MHz divided in 2048 channels and 2 polarisations. The central frequency was set at 1417 MHz resulting in an HI velocity coverage from -100 to 1500 km s⁻¹, with a channel width of 0.82 km s⁻¹. The beam size is 14.1' or 18 kpc at a radial distance of 4.3 Mpc. In MX mode only the seven inner-most horns of the multibeam detectors are used. At all times, one of the beams was kept on-source while the six others observed adjacent sky to provide bandpass calibration, alternating the on-source beam every two minutes. The total integration times ranged from 350 to 650 minutes (see Table 2).

These data were reduced with the LiveData data reduction pipeline. The median of the Tukey-smoothed bandpass was used for calibration and the data were gridded with Gridzilla after averaging the two polarisations. LiveData and Gridzilla are part of the AIPS++ software package. The *mbspect* robust polynomial fitting algorithm from the MIRIAD software package was used to fit low order polynomials and subtract residual baseline ripples.

³The Parkes telescope is part of the Australia Telescope, which is funded by the Commonwealth of Australia for operation as a National Facility managed by the CSIRO.

Table 1: Position and optical parameters of the sample

Galaxy	Type	R.A. (J2000)	Dec. (J2000)	D^a (Mpc)	m_B (mag)	A_B (mag)	v_\odot (km s ⁻¹)	References
ESO219-G010	dE	12 56 10	-50 08 38	4.79±0.43 <i>s</i>	16.42±0.16	0.957	...	1, 2
ESO269-G037	dIrr	13 03 33	-46 35 06	3.48±0.35 <i>t</i>	16.26	0.574	...	3
[CFC97]Cen6	dIrr	13 05 02	-40 04 58	5.78±0.46 <i>t</i>	16.33	0.436	619±43	4, 5
CenA-dE1	dE	13 12 45	-41 49 57	4.21±0.33 <i>t</i>	17.75±0.11	0.493	...	1, 5
ESO269-G066	dE	13 13 09	-44 53 24	4.05±0.53 <i>s</i>	14.59±0.08	0.401	784±31	1, 2
CenA-dE2	dE/dIrr	13 21 33	-31 52 43	...	18.13±0.18	0.288	...	1
SGC1319.1-4216	dE	13 22 02	-42 32 07	3.87±0.31 <i>t</i>	15.68±0.14	0.665	...	1, 5
[CFC97]Cen8	dIrr/dE	13 22 56	-33 34 22	...	17.65±0.08	0.296	...	1, 4
AM1320-230	dE	13 23 29	-23 23 35	...	17.53±0.08	0.348	...	1
UGCA365	dIrr	13 36 31	-29 14 06	5.18±0.41 <i>t</i>	15.53	0.229	573±1	5, 6
[KK98]208 ^b	dIrr	13 36 35	-29 34 17	4.68±0.42 <i>t</i>	14.3	0.192	...	3
AM1339-445	dE	13 42 05	-45 12 18	3.53±0.31 <i>s</i>	16.32±0.1	0.477	...	2, 7
CenA-dE3	dE	13 46 00	-36 20 15	...	17.41±0.15	0.266	...	1
AM1343-452	dE	13 46 16	-45 41 05	3.73±0.32 <i>s</i>	17.57±0.11	0.522	...	1, 2
CenA-dE4	dE	13 46 40	-29 58 41	...	17.60±0.14	0.260	...	1
ESO384-G016	dE/dIrr	13 57 01	-35 20 01	4.23±0.11 <i>s</i>	15.11±0.06	0.318	561±32	1, 2
CenA-dE5	dE	14 30 05	-33 28 45	...	18.43±0.13	0.326	...	1
ESO272-G025	dE/dIrr	14 43 25	-44 42 18	...	14.77	0.694	624±10	3, 4

Note. — Units of right ascension are hours, minutes, and seconds, and units of declination are degrees, arcminutes, and arcseconds (J2000.0).

^aThe distance values marked with *t* denotes a measurement using the tip of the red giant branch method and *s* is used for the surface brightness fluctuation method.

^b[KK98]208 was not explicitly targetted but was in the field of view of UGCA365.

References. — A_B : Schlegel et al. (1998); D , m_B : (1) Jerjen et al. (2000a); (2) Jerjen et al. (2000b); (3) Karachentsev et al. (2002); (4) CFC97; (5) Karachentsev et al. (2006); (6) Huchtmeier et al. (2003); (7) Rejkuba et al. (2006)

2.3. ATCA observations

The Australia Telescope Compact Array (ATCA)⁴ was used to obtain HI line maps and spectra in the direction of the 13 galaxies: ESO269-G037, [CFC97]Cen8, AM1339-445 and ESO384-G016 with the 1.5A array configuration, [CFC97]Cen6 and CenA-dE5 with the 750D configuration, ESO219-G010, CenA-dE2, AM1320-230 and CenA-dE3 using the EW367 configuration and SGC1319.1-4216, UGCA365 and ESO272-G025 with the EW352 configuration. In addition, observations in the direction of [CFC97] Cen5 were also conducted but are not presented here. This galaxy is a background spiral, not associated with the CenA group (Bouchard et al. 2004).

The arrays were chosen so that the final synthesised beam would encompass a maximum of the anticipated flux structure while not being much larger. Precisely, it was the different distances to each object and their respective morphological appearances that were taken into account. This was done to avoid over-resolving the sources which would have led to detection difficulties whilst also avoiding the dilution of the HI signal with the surrounding noise. The observations were carried out in 2003 February and March and in 2004 March and April (project C1133).

The FULL_4_1024-128 correlator configuration was employed with the central frequency of 1417 MHz for an HI line velocity coverage from 200 km s⁻¹ to 1000 km s⁻¹ or of 1416 MHz, covering from 400 km s⁻¹ to 1200 km s⁻¹. The spectra were divided in 1024 channels each of 0.82 km s⁻¹. For each observing session the radio continuum source 1934-638 was observed for 10 minutes for use as a flux and bandpass calibrator. A phase calibrator was also observed for typically 5 minutes every 40 minutes of on-source integration. Total integration times ranged between 270 and 650 minutes (See Table 2).

The data were reduced with the MIRIAD software package using standard procedures. The continuum was fitted and subtracted using a low order polynomial. Each data cube was produced using “natural” weighting of baselines, CLEANed and RESTORed to a Gaussian beam of the same size as the main lobe of the synthesized beam.

Table 2: The 21 cm observation integration time and derived physical parameters

Galaxy	Telescope	T_{int} (min)	S_{HI} (Jy km s ⁻¹)	M_{HI} (10 ⁵ M_{\odot})	v_{\odot} (km s ⁻¹)	σ_v (km s ⁻¹)	$M_{\text{HI}}/L_{\text{B}}$ ($M_{\odot}L_{\odot,B}^{-1}$)
ESO219-G010	ATCA	288	< 0.120	< 6.5	< 0.03
ESO269-G037	ATCA	280	0.14±0.02	4±1	743.8±2.1	9.5±1.9	0.040±0.007
[CFC97]Cen6	ATCA	651	5.31±0.21	420±70	614.2±0.8	12.1±0.8	1.8±0.2
CenA-dE1	PKS	352	< 0.038	< 1.6	< 0.05
ESO269-G066	PKS	651	< 0.026	< 1.0	< 0.002
CenA-dE2	ATCA	271	< 0.118	< 5.1	< 0.24
SGC1319.1-4216	ATCA	614	< 0.081	< 2.9	< 0.01
[CFC97]Cen8	ATCA	287	< 0.126	< 5.5	< 0.17
AM1320-230	ATCA	287	< 0.113	< 4.9	< 0.13
UGCA365	ATCA	540	2.82±0.08	180±30	571.4±0.7	12.7±0.7	0.56±0.05
[KK98]208	ATCA	540	< 0.80	< 41	< 0.05
AM1339-445	ATCA	270	< 0.180	< 5.3	< 0.06
CenA-dE3	ATCA	300	< 0.112	< 4.9	< 0.12
AM1343-452	PKS	422	< 0.041	< 1.3	< 0.04
CenA-dE4	PKS	352	< 0.038	< 1.7	< 0.05
ESO384-G016	ATCA	282	1.04±0.18	44±8	502.9±2.4	8.3±2.0	0.13±0.02
CenA-dE5	ATCA	529	< 0.078	< 3.4	< 0.20
ESO272-G025	ATCA	605	1.52±0.08	70±20	629.2±0.9	10.8±0.9	0.10±0.01

3. Results and H I properties

Our program has detected H I emission in five galaxies: the dIrr ESO269-G037, the dIrr [CFC97]Cen6, the dIrr UGCA365, the dE/dIrr ESO384-G016 and the dE/dIrr ESO272-G025. Line emission maps can be found in Figures 2 and 3; the spectra in Figure 4. Of the 11 galaxies that were not detected, two are of mixed morphology: CenA-dE2 and [CFC97]Cen8 while one is a dIrr: [KK98]208. The rest are early-type dwarfs.

In Table 2 we compile the H I detection parameters or upper-limits on the H I content. For each galaxy, we list the telescope that was used and the total on-source integration time, T_{int} in minutes. For the detected galaxies, the heliocentric radio-velocities V_{\odot} , and velocity dispersions σ_V of the gas are listed. The total H I flux, in Jy km s⁻¹, is given by:

$$S_{\text{HI}} = \int S_v dv \quad (1)$$

where S_v is the flux value within each channel of velocity width dv . The H I mass M_{HI} , in solar units M_{\odot} , was calculated using the standard formula:

$$M_{\text{HI}} = 2.356 \times 10^5 D^2 S_{\text{HI}} \quad (2)$$

where D is the radial distance in Mpc. When D was unavailable from the literature, a value of 4.3 ± 0.7 Mpc was adopted, which corresponds to the mean and standard deviation of the distances to all galaxies in the CenA group (Karachentsev et al. 2006).

The H I mass to blue luminosity ratio $M_{\text{HI}}/L_{\text{B}}$, in solar units $M_{\odot}L_{\odot,\text{B}}^{-1}$ is:

$$M_{\text{HI}}/L_{\text{B}} = 1.5 \times 10^{-7} 10^{0.4(m_{\text{B}}-A_{\text{B}})} S_{\text{HI}} \quad (3)$$

in which m_{B} is the apparent integrated B-band magnitude of the object and A_{B} is the B-band Galactic extinction value along the line of sight (see Table 1). The absolute magnitude of the sun was taken as $M_{\odot,\text{B}} = 5.5$ (Bessell et al. 1998). The quoted errors are the results of quadratic error propagation and, when no error were mentioned for m_{B} , these values were taken as ± 0.1 mag.

Where the galaxies were not detected, Table 2 lists upper-limits for S_{HI} , M_{HI} , and $M_{\text{HI}}/L_{\text{B}}$. These upper-limits were calculated with the same above equations but using a value of S_v equal to three times the RMS in the spectra integrated over 10 km s⁻¹. The RMS was typically ~ 4 mJy beam⁻¹ in ATCA observations and ~ 1 mJy beam⁻¹ in Parkes data.

⁴The Australia Telescope Compact Array is part of the Australia Telescope, which is funded by the Commonwealth of Australia for operation as a National Facility managed by CSIRO.

We should note, however, that while ESO269-G066 is listed as not detected in Table 2, it contains a prominent HI feature in its spectrum at $v_{\odot} = 231 \pm 1 \text{ km s}^{-1}$ with $S_{\text{HI}} \sim 0.33 \text{ Jy km s}^{-1}$ (Figure 5). This feature was not reported by Beaulieu et al. (2006) who observed the same object with the Green Bank Telescope, covering a heliocentric velocity range from 600 to 1000 km s^{-1} ; they have placed an upper-limit of $M_{\text{HI}} < 1.6 \times 10^6 M_{\odot}$ (corrected to a distance of 4.05 Mpc). The optical velocity of this object was established to be $v_{\odot} = 784 \pm 31 \text{ km s}^{-1}$, measured from Balmer absorption lines (Jerjen et al. 2000b). It therefore seems unlikely that this HI feature is associated with the dwarf. A systemic velocity of 231 km s^{-1} would also be inconsistent with a CenA group association, most other objects have velocities greater than 500 km s^{-1} . Inspection of the High Velocity Cloud catalog (Putman et al. 2002) reveals many HVCs in the vicinity of ESO269-G066 at $v_{\odot} \sim 200 \text{ km s}^{-1}$ and one may have been caught in the 14' beam of the Parkes telescope. We conclude that no HI is associated with this galaxy, which therefore has $M_{\text{HI}} < 10^5 M_{\odot}$.

4. Analysis

4.1. Early-type dwarfs

The first interesting result from our HI study that should be pointed out is that none of the ten observed dwarfs classified as dE have been detected in HI. The M_{HI} upper-limits range between $1.0 - 6.5 \times 10^5 M_{\odot}$ and the $M_{\text{HI}}/L_{\text{B}}$ upper-limits are between $0.002 - 0.20 M_{\odot} L_{\odot, \text{B}}^{-1}$. To understand the implications of the $M_{\text{HI}}/L_{\text{B}}$ results, one should consider two extreme examples: CenA-dE5 and ESO269-G066. While both have roughly similar HI mass upper-limits, $M_{\text{HI}} = 3.4 \times 10^5 M_{\odot}$ and $M_{\text{HI}} = 1.0 \times 10^5 M_{\odot}$, respectively, they have very different $M_{\text{HI}}/L_{\text{B}}$ ratios.

CenA-dE5 is the faintest galaxy of our sample and has an absolute magnitude $M_{\text{B}} = -10.1$ (for an assumed distance of 4.3 Mpc). Although this object is brighter than some Local Group dwarfs (e. g., Ursa Minor, $M_{\text{B}} = -7.6$ Mateo 1998), it is amongst the faintest known galaxies in the local universe. It has $M_{\text{HI}}/L_{\text{B}} < 0.2 M_{\odot} L_{\odot, \text{B}}^{-1}$. At the bright end of our optical luminosity distribution, ESO269-G066 has $M_{\text{B}} = -13.8$ and $M_{\text{HI}}/L_{\text{B}} < 2 \times 10^{-3} M_{\odot} L_{\odot, \text{B}}^{-1}$.

As a first approximation, both these galaxies can be considered as being dominated by an old and metal poor stellar population (see Jerjen et al. 2000b). The mass loss expected from the evolution of such a population is of the order of $0.1 M_{\odot} L_{\odot, \text{B}}^{-1}$ over a Hubble time (Bouchard et al. 2005). It becomes immediately obvious that while the $M_{\text{HI}}/L_{\text{B}}$ upper-limit for CenA-dE5 does not exclude such mass loss material being in the form of HI, it is very

stringent on the state of ESO269-G066. In this latter case, any neutral gas build-up is, at best, insignificant. The upper-limit on $M_{\text{HI}}/L_{\text{B}}$ actually requires that the ISM in this galaxy is either completely ionised or, more likely, has been regularly and thoroughly swept out of the dwarf. For comparison purposes, the Local Group dE galaxies NGC185 and NGC205, both satellites of M31 have $M_{\text{HI}}/L_{\text{B}} = 4 \times 10^{-3}$ and $3 \times 10^{-3} M_{\odot} L_{\odot, \text{B}}^{-1}$, respectively (Young & Lo 1997).

4.2. Mixed-type dwarfs

Of the four mixed-type dwarfs that were observed, two were detected in HI: the dE/dIrr ESO384-G016 with $M_{\text{HI}} = (4.4 \pm 0.8) \times 10^6 M_{\odot}$, $M_{\text{HI}}/L_{\text{B}} = 0.13 \pm 0.02 M_{\odot} L_{\odot, \text{B}}^{-1}$ and the dE/dIrr ESO272-G025 with $M_{\text{HI}} = (7 \pm 2) \times 10^6 M_{\odot}$ and $M_{\text{HI}}/L_{\text{B}} = 0.10 \pm 0.01 M_{\odot} L_{\odot, \text{B}}^{-1}$. The two others, the dE/dIrr CenA-dE2 and the dIrr/dE [CFC97]Cen8 have upper-limits of $M_{\text{HI}} < 5.1 \times 10^5 M_{\odot}$, $M_{\text{HI}}/L_{\text{B}} < 0.24 M_{\odot} L_{\odot, \text{B}}^{-1}$ and $M_{\text{HI}} < 5.5 \times 10^5 M_{\odot}$, $M_{\text{HI}}/L_{\text{B}} < 0.17 M_{\odot} L_{\odot, \text{B}}^{-1}$, respectively.

We note that Beaulieu et al. (2006) previously observed ESO384-G016 with the ATCA and found $M_{\text{HI}} = (5.6 \pm 0.3) \times 10^6 M_{\odot}$, in good agreement with our result. They had a longer integration time which resulted in a higher signal-to-noise ratio and, most probably, a more accurate result. These authors have also found that single dish observation yielded $M_{\text{HI}} = (6.5 \pm 0.1) \times 10^6 M_{\odot}$, which highlights the fact that approximately 25% of the flux resides in scales inaccessible to our array configuration. We also note that ESO272-G025 had previously been detected in H α but not in HI (Côté et al. 1997).

At first sight, this situation may seem contrasting to that of both the Local Group and the Sculptor group where all mixed-morphology galaxies have been detected in HI. On closer inspection, however, Local Group mixed-morphology dwarfs have $M_{\text{HI}}/L_{\text{B}}$ between 0.21 and $1.4 M_{\odot} L_{\odot, \text{B}}^{-1}$ (St-Germain et al. 1999; Blitz & Robishaw 2000; Bouchard et al. 2006), while in the Sculptor group these objects have $M_{\text{HI}}/L_{\text{B}}$ between 0.08 and $0.18 M_{\odot} L_{\odot, \text{B}}^{-1}$ (Bouchard et al. 2005). The $M_{\text{HI}}/L_{\text{B}} < 0.24 M_{\odot} L_{\odot, \text{B}}^{-1}$ constraint imposed on the two non-detected CenA dwarfs does not exclude HI contents similar to those of Sculptor mixed morphology dwarfs.

4.3. Late-type dwarfs

It comes with some surprise that not all observed late type dwarfs were detected in HI. While ESO269-G037, [CFC97]Cen6 and UGCA365 all have considerable amounts of ISM,

$M_{\text{HI}} = (4 \pm 1) \times 10^5 M_{\odot}$ and $M_{\text{HI}}/L_{\text{B}} = 0.04 \pm 0.02 M_{\odot} L_{\odot, \text{B}}^{-1}$, $M_{\text{HI}} = (42 \pm 7) \times 10^6 M_{\odot}$ and $M_{\text{HI}}/L_{\text{B}} = 1.81 \pm 0.08 M_{\odot} L_{\odot, \text{B}}^{-1}$ and $M_{\text{HI}} = (18 \pm 3) \times 10^6 M_{\odot}$ and $M_{\text{HI}}/L_{\text{B}} = 0.56 \pm 0.02 M_{\odot} L_{\odot, \text{B}}^{-1}$, respectively, [KK98]208 was not detected with limits of $M_{\text{HI}} < 4.1 \times 10^6 M_{\odot}$ and $M_{\text{HI}}/L_{\text{B}} < 0.05 M_{\odot} L_{\odot, \text{B}}^{-1}$. From empirical evidence, we would have expected most dIrr galaxies to have $M_{\text{HI}}/L_{\text{B}}$ between 0.1 and $10 M_{\odot} L_{\odot, \text{B}}^{-1}$ at $M_{\text{B}} = -14$ (Warren et al. 2006).

The galaxy [KK98]208 was added to the sample after the observations as it resides only 30' away from UGCA365. The upper-limit for S_{HI} and correspondingly for M_{HI} is higher than for any other galaxy of our sample (see Table 2) and, with $M_{\text{B}} = -14.2$, this galaxy is optically brighter than most other objects in our sample. This makes the $M_{\text{HI}}/L_{\text{B}}$ ratio limit of $0.05 M_{\odot} L_{\odot, \text{B}}^{-1}$ surprisingly low for a dIrr. No dwarf galaxy in the Koribalski et al. (2004) sample has values this low (also see Warren et al. 2006).

[KK98]208 also happens to share a similar line of sight to the spiral NGC5236 (M83), which has HI extending up to and beyond the spatial position of [KK98]208. Huchtmeier et al. (2000) claim to have detected the dwarf at $V_{\odot} = 400 \text{ km s}^{-1}$, but this detection is confused with the 21 cm signal from NGC5236. The northern spiral arm of NGC5236 is easily detected in our data at the velocity mentioned by Huchtmeier et al. (2000), but there are no signs of kinematically-decoupled HI emission near the dwarf. It is also worth noting that Karachentsev et al. (2002) found, in the colour-magnitude diagram of this dwarf, a predominantly old stellar population typical of a dE, in disagreement with its irregular morphology (KK98). However, its extreme low surface brightness makes classification on morphological grounds intrinsically difficult (see Figure 3 from Karachentsev et al. 2002, online material). Both the stellar population and the HI properties of this object clearly favour an early-type classification.

It is also interesting to note that the dIrr galaxy ESO269-G037 has $M_{\text{HI}}/L_{\text{B}} = 0.04 M_{\odot} L_{\odot, \text{B}}^{-1}$. This value is low for a dwarf of late-morphology. Based on stellar photometry, Karachentsev et al. (2002) argued that this galaxy should actually be considered as a dSph. The object may also harbour a small population of blue stars, which would be consistent with the HI result.

4.4. HI displacement and ram pressure

Angular displacement of the HI with respect to the optical center is observed in a number of dwarf galaxies. In the Local Group, this is seen in two of the five mixed-morphology galaxies, Phoenix and LGS 3 (St-Germain et al. 1999; Gallart et al. 2001; Robishaw et al. 2002), while in the Sculptor group, this is likely the case for two of the three investigated mixed-morphology dwarfs. In the CenA group, we only detect a possible HI displacement in

ESO269-G037, but the low signal to noise of the map presented in Figure 2 makes it difficult to accurately determine if the gas is really offset with respect to the optical centre.

We do, however, detect a discrepancy between the H I velocity $v_{\odot} = 502.9 \pm 2.4$ km s⁻¹ (consistent with the measurement of Beaulieu et al. 2006) and the optical velocity $v_{\odot} = 561 \pm 32$ km s⁻¹ (Jerjen et al. 2000b) for ESO384-G016. While Beaulieu et al. (2006) argued that the H I velocity is probably more accurate than the optical, they also suggested that, based on the H I distribution, this galaxy may be experiencing ram pressure while falling into the group. Jerjen et al. (2000b) noted that this galaxy has an old and metal-poor stellar population and the optical spectra shows no sign of current star formation. Ram pressure stripping may be able to displace the gas while keeping it with a smooth distribution (Gallart et al. 2001), not necessarily triggering star formation. Moreover, the H I is at a lower velocity than the optical, a situation we would expect if ESO384-G016, at $D = 4.2$ Mpc, is falling onto NGC5236 at $D = 5.1$ Mpc (Karachentsev et al. 2006). Since the mechanism causing this offset is unlikely to be aligned with the radial direction, the velocity difference should also have produced a measurable angular offset if it is the result of a gentle ‘push’ or have produced star forming regions if the event was more violent. Alternatively, it may be that the gas is being compressed and star formation is about to start. This object would then evolve back toward a late-type morphology. The spectral information available for this object is of too low signal-to-noise. Further observations will be required to investigate whether the H I line shape may have been influenced by ram pressure.

The Eastern H I extension detected by Beaulieu et al. (2006) in ESO384-G016 is similar to the north-western H I extension of UGCA365 (Figure 2). This latter galaxy is situated ~ 81 kpc three dimensional distance from NGC5236 (M83), a separation reminiscent of that of the Large and Small Magellanic Clouds to the Milky Way. It is possible that this object is experiencing ram pressure and tidal stripping as it travels on its orbit around M83.

4.5. CenA environment and dwarf evolution

The CenA group is a relatively high density environment providing external conditions which can influence the evolution of its group members. In fact, one of the most important features of this environment is the presence of the active galaxy NGC5128 (CenA). The radio-lobes of NGC5128 may be dramatically affecting nearby objects (see Figure 6). These regions of hot ionised plasma measure 9° (~ 600 kpc) in the north-south direction and 3° (~ 200 kpc) east-west (e.g., Junkes et al. 1993). This may have affected the evolution of nearby dwarfs.

There are six galaxies projected near NGC5128. These include the three early type dwarfs, CenA-dE1, SGC1319.1-4216 and ESO269-G066, none of which were detected in HI (Table 2). The three other objects are gas rich (CFC97, Koribalski et al. 2004). The spiral ESO270-G017 (also known as Fourcade-Figueroa) and the irregular NGC5237 are believed to be the remnants of a close interaction between a spiral galaxy and NGC5128, which may have been at the origin of the latter’s observed dust lane (Dottori & Fourcade 1973; Thomson 1992). Finally, the dIrr ESO324-G024 is known to have H α and H β emission, both signs of active star formation (Lee et al. 2003).

In the case of ESO269-G066, there is a good agreement in radial distance with NGC5128: $D = 3.84 \pm 0.35$ Mpc, (Rejkuba 2004) compared to 4.05 ± 0.53 Mpc for ESO269-G066 (Jerjen et al. 2000b). The relative line of sight velocity is $\Delta v \sim 240$ km s $^{-1}$ ($v_{\odot}(\text{NGC5128}) = 543 \pm 2$ km s $^{-1}$, Israel 1998). It is possible that the orbit of the dwarf brings it regularly through the lobes of NGC5128. The very low limit on the HI mass to light ratio of ESO269-G066, $M_{\text{HI}}/L_{\text{B}} < 2 \times 10^{-3}$, and the evidence that it contains mostly old and metal poor stars (Jerjen et al. 2000b) suggests that these passages through the lobes may be ‘actively cleansing’ the dwarf of any traces of accumulated gas, probably by means of intensified ram pressure and, possibly, heating due to the higher X-ray radiation field in the plasma. In any case, this would prevent any further star formation. The other early-type dwarfs CenA-dE1 and SGC1319.1-4216 may be in similar positions, however, independent measurement of their distances are required to reveal the likeliness of these objects going through the lobes.

To investigate this intensified ram pressure, we compare in Figure 7 the M_{HI} and L_{B} values of all known galaxies from the CenA and Sculptor group. It becomes apparent that the different global environments, and not just the direct proximity to an AGN, acted differently on the evolution of their respective fainter members. When compared to the CenA group, Sculptor seems to be lacking both low and high HI mass objects in the range $-14 < M_{\text{B}} < -11$. It provides much more of a continuum of HI mass towards fainter objects than the CenA group does; the latter seems to have more of a dichotomy between the HI rich and HI deficient objects. Precisely, Sculptor has a single galaxy with no detected HI and $M_{\text{HI}}/L_{\text{B}} < 0.05 M_{\odot}/L_{\odot,\text{B}}$, while, on the one hand, CenA has at least 16 galaxies that were not detected in HI and at least eight with $M_{\text{HI}}/L_{\text{B}} < 0.05 M_{\odot}/L_{\odot,\text{B}}$. The CenA environment seems much more efficient in removing gas from dwarfs than the Sculptor one. On the other hand CenA also has a much more prominent population of galaxies with $1 < M_{\text{HI}}/L_{\text{B}} < 10 M_{\odot}/L_{\odot,\text{B}}$ than Sculptor.

Gunn & Gott (1972) determined that the ISM of a galaxy will be stripped away by ram pressure if

$$\rho_{\text{IGM}} \gtrsim \rho_{\text{ISM}} \left(\frac{\sigma_{\text{ISM}}}{v_p} \right)^2 \quad (4)$$

for a galaxy with an ISM of density ρ_{ISM} and velocity dispersion of σ_{ISM} , travelling at a velocity v_p through an intergalactic medium of density ρ_{IGM} . By adopting $\sigma_{\text{ISM}} = 10 \text{ km s}^{-1}$, a value typical for the studied dwarfs (e. g., Mateo 1998; Bouchard et al. 2005) and taking a value of $v_p \sim 300 \text{ km s}^{-1}$, we find that if $\rho_{\text{IGM}} \gtrsim 10^{-3} \rho_{\text{ISM}}$, ram pressure will eventually remove all the gas in a low mass dwarf. In the case of the dE ESO269-G066 the ISM density is $\rho_{\text{ISM}} < 10^{-2} \text{ cm}^{-3}$ ($M_{\text{HI}} < 10^5 M_{\odot}$ inside a presumed radius of 1 kpc). This value is much lower than that of the dIrr ESO324-G024, where $\rho_{\text{ISM}} = 15 \text{ cm}^{-3}$ ($M_{\text{HI}} = 1.5 \times 10^8 M_{\odot}$, CFC97, inside a radius of 1 kpc). An IGM density of the order of $\sim 10^{-3} \text{ cm}^{-3}$ would therefore strip away any gas accumulation in ESO269-G066 but otherwise leave ESO324-G024 intact. These values for ρ_{IGM} are consistent with the values measured by X-ray observations of NGC5128 (Cooke et al. 1978; Feigelson et al. 1981) and of loose galaxy groups (Mulchaey et al. 1996; Helsdon & Ponman 2000).

Figure 7 shows that, for the faint objects of the CenA group ($M_B > -13$), there seems to be a threshold in HI masses at values of $M_{\text{HI}} \sim 10^7 M_{\odot}$. All objects below this value have at least a factor of 10 less HI than the ones above. In fact, there is only one detected galaxy below this limit: the dIrr ESO269-G037 with $M_{\text{HI}} = 4 \times 10^5 M_{\odot}$. It seems that the dwarfs situated above the threshold have kept their HI while the ones below are efficiently swept clean of ISM.

Assuming that the $10^7 M_{\odot}$ threshold indeed exists, we can redefine the morphological classification of dwarf galaxies based on HI properties. In the $M_B > -14$ regime of the CenA group, there are 13 late-type dwarfs ($M_{\text{HI}} \gtrsim 10^7 M_{\odot}$) which may keep their ISM for a long period of time. These are objects like [CFC97]Cen6 ($M_{\text{HI}}/L_B = 1.8$). They have an important untapped and stable potential for further star formation. There is also a single detected transition-type galaxy (ESO269-G037) that might currently be losing its ISM through ram pressure stripping. Finally, there are 12 early-type dwarfs candidates, where no ISM has been detected. Much like Ursa Minor in the Local Group or Scl-dE1 in the Sculptor group, their lack of ISM prohibits any further star formation and they have reached their final evolutionary state. If any of the latter type would contain HI, it should be considered a transition-type object because such low HI content would be short lived and prone to ram pressure stripping. The current sensitivity of HI observations allows to distinguish the late-type dwarfs but does not allow a differentiation between the early and transition type dwarfs at the distance of the CenA group (4.3 Mpc).

Finally, we note that the present investigation has targeted some of the faintest known members of the CenA group. The HI survey for these galaxies, i. e., fainter than $M_B > -14$, is now complete to an HI mass of $10^6 M_{\odot}$. However, it is most likely that not all dwarf galaxies of the CenA or Sculptor groups have been found to date. For example, in the Local

Group, 10 of the ~ 40 members are fainter than $M_B > -10$. In the CenA group there are only four galaxies of the ~ 45 galaxies that are this faint. The advent of next generation optical surveys will probably uncover new group members. These future discoveries and H I followup work will give an even better insight into the properties for galaxies at the faint end of the luminosity function, for different environments.

5. Conclusions

We have presented Parkes single dish and ATCA interferometric H I observations of 18 low luminosity dwarf galaxies belonging to the CenA group, with an emphasis on early-type dwarfs. This was done in order to identify objects with H I reservoirs and, therefore, potential for further star formation. As a result, we can constrain dwarf galaxy evolution scenarios by providing a thorough analysis of a nearby dense environment.

The main conclusions can be summarised as follow:

1. Of the 18 observed dwarfs, five were detected: three were late-type dwarfs and two were of mixed-morphology. None of the early-type objects were found to contain H I. The detection limits on all non-detected early and mixed-type objects are in the range from $M_{\text{HI}} < 10^5 M_\odot$ to $M_{\text{HI}} < 6.5 \times 10^5 M_\odot$, $M_{\text{HI}}/L_B < 0.24 M_\odot L_{\odot,B}^{-1}$.
2. Unlike the Local Group and the Sculptor group where all mixed-morphology dwarfs are detected in H I, only two of the four CenA mixed-type dwarfs are detected. However, the limits on the non-detections do not exclude H I contents similar to those of other mixed-type dwarfs in the Sculptor or Local Group.
3. The H I masses of the detected objects range from $4 \times 10^5 M_\odot$ to $4.2 \times 10^7 M_\odot$, the H I mass to luminosity ratios range from $0.04 M_\odot L_{\odot,B}^{-1}$ to $1.81 M_\odot L_{\odot,B}^{-1}$. The H I velocities vary between 500 and 750 km s⁻¹, compatible with the expected velocities for the CenA group members.
4. There is a gap in H I properties for low mass CenA dwarf galaxies. These objects either have H I masses $M_{\text{HI}} > 10^7 M_\odot$ or are not detected, consequently must have $M_{\text{HI}} \lesssim 10^6 M_\odot$. This gap can be explained by the ram pressure exerted by an IGM of density $\rho_{\text{IGM}} \sim 10^{-3} \text{ cm}^{-3}$.
5. The dE ESO269-G066 has $M_{\text{HI}}/L_B < 0.002 M_\odot L_{\odot,B}^{-1}$, which is much lower than the value expected from the gas accumulated through normal stellar evolution. The orbit of the dwarf may bring it regularly into the radio-lobes of the the active galaxy NGC5128

constantly sweeping it free of gas. Other galaxies may have been similarly affected by the presence of NGC5128.

6. An H I distribution similar to what is expected from the effects of mild ram pressure is found in UGCA365, ESO384-G016 and, possibly, in ESO269-G037.

Further investigation of denser environments, such as nearby clusters, with equally low H I detection limits are required to establish whether the gap in H I properties of dwarf galaxies is common. If this is the case, it may have profound implications on our understanding of dwarf galaxy evolution.

We would like to thank Sylvie Beaulieu, Geoff Bicknell and Erwin deBlok for insightful discussions. We also thank Norbert Junkes who kindly provided the data for Figure 6 and the referee for the much appreciated comments. We acknowledge the support from the Australian Research Council through Discovery Project Grant DP0343156. This research has made use of the NASA/IPAC Extragalactic Database (NED) which is operated by the Jet Propulsion Laboratory, California Institute of Technology, under contract with the National Aeronautics and Space Administration. This work is partly based on photographic data obtained using The UK Schmidt Telescope. The UK Schmidt Telescope was operated by the Royal Observatory Edinburgh, with funding from the UK Science and Engineering Research Council, until 1988 June, and thereafter by the Anglo-Australian Observatory. Original plate material is copyrighted by the Royal Observatory Edinburgh and the Anglo-Australian Observatory. The plates were processed into the present compressed digital form with their permission. The Digitized Sky Survey was produced at the Space Telescope Science Institute under US Government grant NAG W-2166.

REFERENCES

- Babusiaux, C., Gilmore, G., & Irwin, M. 2005, MNRAS, 359, 985
- Banks, G. D., Disney, M. J., Knezek, P. M., Jerjen, H., Barnes, D. G., Bhatal, R., de Blok, W. J. G., Boyce, P. J., Ekers, R. D., Freeman, K. C., Gibson, B. K., Henning, P. A., Kilborn, V., Koribalski, B., Kraan-Korteweg, R. C., Malin, D. F., Minchin, R. F., Mould, J. R., Oosterloo, T., Price, R. M., Putman, M. E., Ryder, S. D., Sadler, E. M., Staveley-Smith, L., Stewart, I., Stootman, F., Vaile, R. A., Webster, R. L., & Wright, A. E. 1999, ApJ, 524, 612
- Barnes, D. G., Staveley-Smith, L., de Blok, W. J. G., Oosterloo, T., Stewart, I. M., Wright, A. E., Banks, G. D., Bhatal, R., Boyce, P. J., Calabretta, M. R., Disney, M. J.,

- Drinkwater, M. J., Ekers, R. D., Freeman, K. C., Gibson, B. K., Green, A. J., Haynes, R. F., te Lintel Hekkert, P., Henning, P. A., Jerjen, H., Juraszek, S., Kesteven, M. J., Kilborn, V. A., Knezek, P. M., Koribalski, B., Kraan-Korteweg, R. C., Malin, D. F., Marquarding, M., Minchin, R. F., Mould, J. R., Price, R. M., Putman, M. E., Ryder, S. D., Sadler, E. M., Schröder, A., Stootman, F., Webster, R. L., Wilson, W. E., & Ye, T. 2001, *MNRAS*, 322, 486
- Beaulieu, S. F., Freeman, K. C., Carignan, C., Lockman, F. J., & Jerjen, H. 2006, *AJ*, 131, 325
- Bessell, M. S., Castelli, F., & Plez, B. 1998, *A&A*, 333, 231
- Binggeli, B., Tammann, G. A., & Sandage, A. 1987, *AJ*, 94, 251
- Binggeli, B., Tarenghi, M., & Sandage, A. 1990, *A&A*, 228, 42
- Blitz, L., & Robishaw, T. 2000, *ApJ*, 541, 675
- Bouchard, A., Carignan, C., & Mashchenko, S. 2003, *AJ*, 126, 1295
- Bouchard, A., Carignan, C., & Staveley-Smith, L. 2006, *AJ*, 131, 2913
- Bouchard, A., Da Costa, G. S., & Jerjen, H. 2004, *PASP*, 116, 1031
- Bouchard, A., Jerjen, H., Da Costa, G. S., & Ott, J. 2005, *AJ*, 130, 2058
- Buyle, P., De Rijcke, S., Michielsen, D., Baes, M., & Dejonghe, H. 2005, *MNRAS*, 360, 853
- Carignan, C., Beaulieu, S., Côté, S., Demers, S., & Mateo, M. 1998, *AJ*, 116, 1690
- Conselice, C. J., O’Neil, K., Gallagher, J. S., & Wyse, R. F. G. 2003, *ApJ*, 591, 167
- Cooke, B. A., Lawrence, A., & Perola, G. C. 1978, *MNRAS*, 182, 661
- Côté, S., Freeman, K. C., Carignan, C., & Quinn, P. J. 1997, *AJ*, 114, 1313
- De Rijcke, S., Dejonghe, H., Zeilinger, W. W., & Hau, G. K. T. 2003, *A&A*, 400, 119
- . 2004, *A&A*, 426, 53
- Dottori, H. A., & Fourcade, C. R. 1973, *A&A*, 23, 405
- Dressler, A. 1980, *ApJ*, 236, 351
- Einasto, J., Saar, E., Kaasik, A., & Chernin, A. D. 1974, *Nature*, 252, 111

- Feigelson, E. D., Schreier, E. J., Delvaille, J. P., Giacconi, R., Grindlay, J. E., & Lightman, A. P. 1981, *ApJ*, 251, 31
- Gallart, C., Martínez-Delgado, D., Gómez-Flechoso, M. A., & Mateo, M. 2001, *AJ*, 121, 2572
- Grebel, E. K. 2001, *Astrophysics and Space Science Supplement*, 277, 231
- Grebel, E. K., Gallagher, J. S., & Harbeck, D. 2003, *AJ*, 125, 1926
- Gunn, J. E., & Gott, J. R. I. 1972, *ApJ*, 176, 1
- Helsdon, S. F., & Ponman, T. J. 2000, *MNRAS*, 315, 356
- Huchtmeier, W. K., Karachentsev, I. D., & Karachentseva, V. E. 2001, *A&A*, 377, 801
- . 2003, *A&A*, 401, 483
- Huchtmeier, W. K., Karachentsev, I. D., Karachentseva, V. E., & Ehle, M. 2000, *A&AS*, 141, 469
- Israel, F. P. 1998, *A&A Rev.*, 8, 237
- Jerjen, H., Binggeli, B., & Freeman, K. C. 2000a, *AJ*, 119, 593
- Jerjen, H., Freeman, K. C., & Binggeli, B. 1998, *AJ*, 116, 2873
- . 2000b, *AJ*, 119, 166
- Junkes, N., Haynes, R. F., Harnett, J. I., & Jauncey, D. L. 1993, *A&A*, 269, 29
- Karachentsev, I. D., Karachentseva, V. E., Huchtmeier, W. K., & Makarov, D. I. 2004, *AJ*, 127, 2031
- Karachentsev, I. D., Sharina, M. E., Dolphin, A. E., Grebel, E. K., Geisler, D., Guhathakurta, P., Hodge, P. W., Karachentseva, V. E., Sarajedini, A., & Seitzer, P. 2002, *A&A*, 385, 21
- Karachentsev, I. D., Tully, R. B., Dolphin, A., Sharina, M., Makarova, L., Makarov, D., Kashibadze, O. G., Karachentseva, V., Sakai, S., Shaya, E. J., & Rizzi, L. 2006, [astro-ph/0603091](https://arxiv.org/abs/astro-ph/0603091)
- Karachentseva, V. E., & Karachentsev, I. D. 1998, *A&AS*, 127, 409
- . 2000, *A&AS*, 146, 359

- Koribalski, B. S., Staveley-Smith, L., Kilborn, V. A., Ryder, S. D., Kraan-Korteweg, R. C., Ryan-Weber, E. V., Ekers, R. D., Jerjen, H., Henning, P. A., Putman, M. E., Zwaan, M. A., de Blok, W. J. G., Calabretta, M. R., Disney, M. J., Minchin, R. F., Bhathal, R., Boyce, P. J., Drinkwater, M. J., Freeman, K. C., Gibson, B. K., Green, A. J., Haynes, R. F., Juraszek, S., Kesteven, M. J., Knezek, P. M., Mader, S., Marquarding, M., Meyer, M., Mould, J. R., Oosterloo, T., O'Brien, J., Price, R. M., Sadler, E. M., Schröder, A., Stewart, I. M., Stootman, F., Waugh, M., Warren, B. E., Webster, R. L., & Wright, A. E. 2004, *AJ*, 128, 16
- Lee, H., Grebel, E. K., & Hodge, P. W. 2003, *A&A*, 401, 141
- Lo, K. Y., Sargent, W. L. W., & Young, K. 1993, *AJ*, 106, 507
- Marcolini, A., Brighenti, F., & D'Ercole, A. 2004, *MNRAS*, 352, 363
- Mashchenko, S., Carignan, C., & Bouchard, A. 2004, *MNRAS*, 352, 168
- Mateo, M. L. 1998, *ARA&A*, 36, 435
- Mayer, L., Governato, F., Colpi, M., Moore, B., Quinn, T., Wadsley, J., Stadel, J., & Lake, G. 2001, *ApJ*, 547, L123
- Moore, B., Katz, N., & Lake, G. 1996, *ApJ*, 457, 455
- Mould, J. R., Bothun, G. D., Hall, P. J., Staveley-Smith, L., & Wright, A. E. 1990, *ApJ*, 362, L55
- Mulchaey, J. S., Davis, D. S., Mushotzky, R. F., & Burstein, D. 1996, *ApJ*, 456, 80
- Olszewski, E. W., Mateo, M., Harris, J., Walker, M. G., Coleman, M. G., & Da Costa, G. S. 2006, *AJ*, 131, 912
- Pedraz, S., Gorgas, J., Cardiel, N., Sánchez-Blázquez, P., & Guzmán, R. 2002, *MNRAS*, 332, L59
- Putman, M. E., de Heij, V., Staveley-Smith, L., Braun, R., Freeman, K. C., Gibson, B. K., Burton, W. B., Barnes, D. G., Banks, G. D., Bhathal, R., de Blok, W. J. G., Boyce, P. J., Disney, M. J., Drinkwater, M. J., Ekers, R. D., Henning, P. A., Jerjen, H., Kilborn, V. A., Knezek, P. M., Koribalski, B., Malin, D. F., Marquarding, M., Minchin, R. F., Mould, J. R., Oosterloo, T., Price, R. M., Ryder, S. D., Sadler, E. M., Stewart, I., Stootman, F., Webster, R. L., & Wright, A. E. 2002, *AJ*, 123, 873
- Read, J. I., & Gilmore, G. 2005, *MNRAS*, 356, 107

- Rejkuba, M. 2004, *A&A*, 413, 903
- Rejkuba, M., da Costa, G. S., Jerjen, H., Zoccali, M., & Binggeli, B. 2006, *A&A*, 448, 983
- Robishaw, T., Simon, J. D., & Blitz, L. 2002, *ApJ*, 580, L129
- Schlegel, D. J., Finkbeiner, D. P., & Davis, M. 1998, *ApJ*, 500, 525
- Simien, F., & Prugniel, P. 2002, *A&A*, 384, 371
- St-Germain, J., Carignan, C., Côté, S., & Oosterloo, T. 1999, *AJ*, 118, 1235
- Thomson, R. C. 1992, *MNRAS*, 257, 689
- Tolstoy, E., Irwin, M. J., Helmi, A., Battaglia, G., Jablonka, P., Hill, V., Venn, K. A., Shetrone, M. D., Letarte, B., Cole, A. A., Primas, F., Francois, P., Arimoto, N., Sadakane, K., Kaufer, A., Szeifert, T., & Abel, T. 2004, *ApJ*, 617, L119
- van den Bergh, S. 1994, *ApJ*, 428, 617
- van Zee, L., Skillman, E. D., & Haynes, M. P. 2004, *AJ*, 128, 121
- Warren, B. E., Jerjen, H., & Koribalski, B. S. 2006, *AJ*, 131, 2056
- Young, L. M., & Lo, K. Y. 1997, *ApJ*, 476, 127

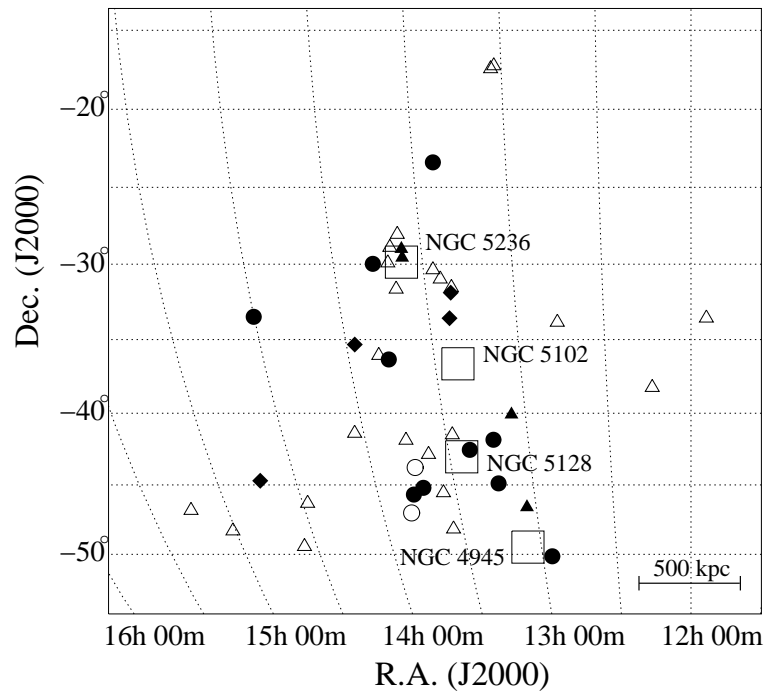


Fig. 1.— Sky distribution of the CenA group galaxies. The large squares mark the position of the major galaxies, while the circles represent early-type dwarfs, triangles for late-type dwarfs and diamonds are used for mixed-morphology dwarfs. Filled symbols represent the observed galaxies.

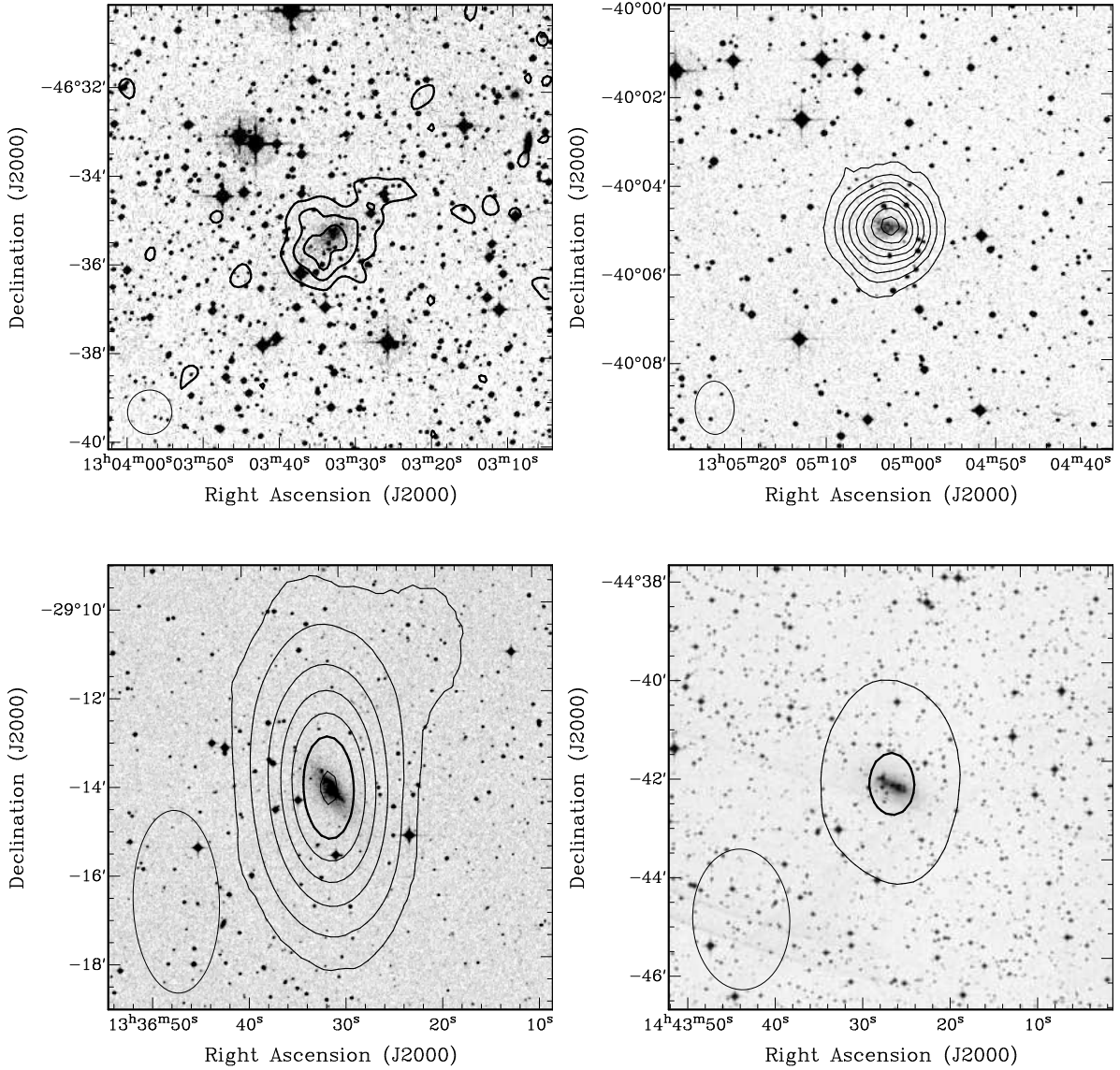


Fig. 2.— HI distribution map (*contours*) overlaid on $10' \times 10'$ DSS images (or $\sim 12\text{kpc} \times 12\text{kpc}$ at an average distance of 4.1 Mpc) of the dIrr ESO269-G037 (top-left), the dIrr [CFC97]Cen06 (top-right), the dIrr UGCA365 (bottom-left) and dE/dIrr ESO272-G025 (bottom-right). The contour levels are from $5 \times 10^{19} \text{ cm}^{-2}$ to $5 \times 10^{20} \text{ cm}^{-2}$ by steps of $5 \times 10^{19} \text{ cm}^{-2}$ except for ESO269-G037 where contours are of 2.5 , 5.0 and $7.5 \times 10^{19} \text{ cm}^{-2}$. The ellipses in the bottom-left corner of each frame is the synthesised beam size: $60'' \times 60''$ for ESO269-G037, $72'' \times 53''$ for [CFC97]Cen6, $247'' \times 117''$ for UGCA365 and $171'' \times 118''$ for ESO272-G025.

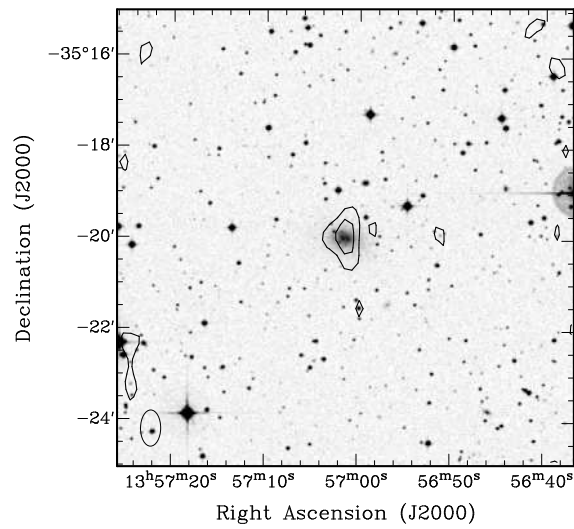


Fig. 3.— HI distribution map (*contours*) overlaid on a $10' \times 10'$ DSS image (or $\sim 12 \text{ kpc} \times 12 \text{ kpc}$ at an average distance of 4.1 Mpc) of the dE/dIrr ESO384-G016. The contour levels are of 1×10^{19} and $2 \times 10^{19} \text{ cm}^{-2}$. The ellipse in the bottom-left corner is the synthesised beam size: $47'' \times 26''$. HI was previously detected in this galaxy by Beaulieu et al. (2006).

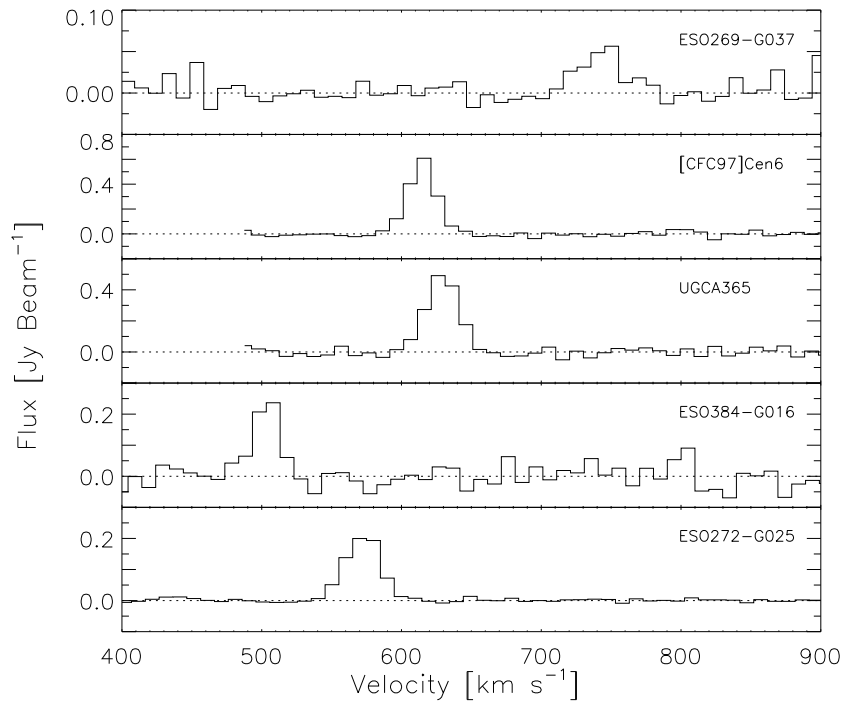


Fig. 4.— ATCA HI spectra for ESO269-G037, [CFC97]Cen06, UGCA365, ESO384-G016 and ESO272-G025. The spectra were binned to a 10 km s^{-1} velocity resolution.

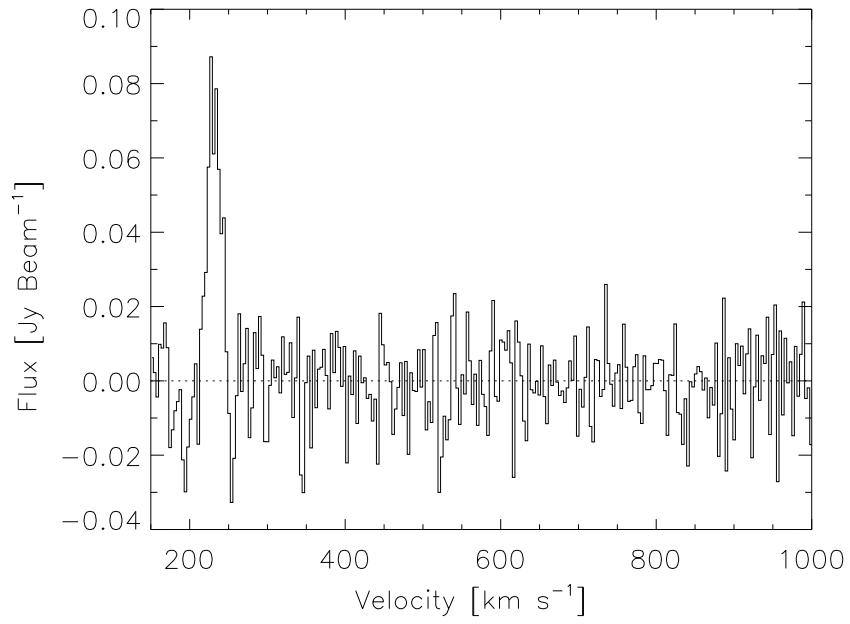


Fig. 5.— Parkes HI spectra for ESO269-G066. The spectra was binned to a 3.3 km s^{-1} velocity resolution.

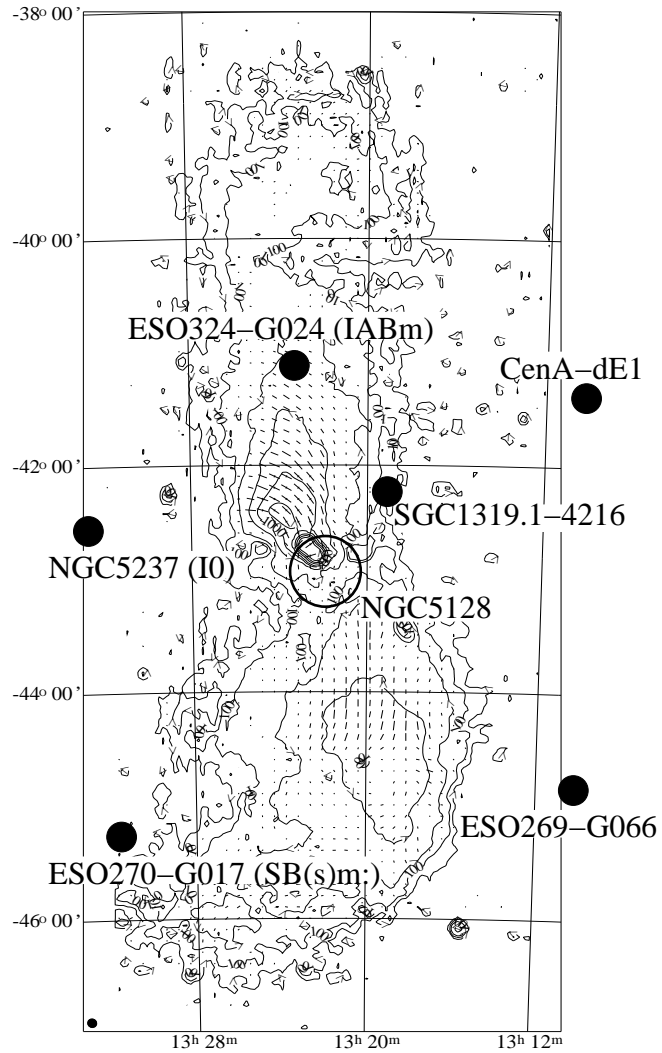


Fig. 6.— The total power radio continuum map around NGC5128 (*open circle*), from Junkes et al. (1993). It is overlaid with the approximate location of six neighbouring galaxies (*filled circles*). The three galaxies ESO324-G024, NGC5237 and ESO270-G017 were not observed.

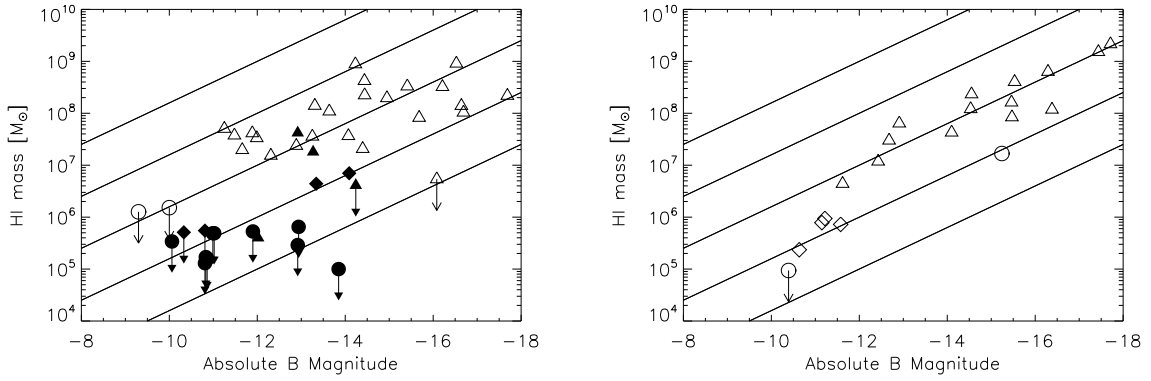


Fig. 7.— HI mass vs. absolute B -band magnitude for early-type dwarfs (*circles*), mixed-type dwarfs (*diamonds*) and late-type dwarfs (*triangles*) of the CenA (*left*) and the Scl (*right*) groups. Solid symbols are the observed galaxies and the other data were taken from Côté et al. (1997); Huchtmeier et al. (2000, 2001); Bouchard et al. (2005); Beaulieu et al. (2006). The diagonal lines show constant $M_{\text{HI}}/L_{\text{B}}$ values of 100, 10, 1, 0.1, 0.01 $M_{\odot}/L_{\odot,\text{B}}$ (*top to bottom*).